J Seismol (2008) 12:53–64
DOI 10.1007/s10950-007-9072-0

ORIGINAL PAPER

Probabilistic aftershock hazard assessment I: numerical testing of methodological features

František Gallovič · Johana Brokešová

Received: 11 May 2006 / Accepted: 31 October 2007 / Published online: 13 December 2007

Abstract Probabilistic aftershock hazard assessment (PAHA, Wiemer, Geoph Res Lett 27:3405–3408, 2000), provided for California within the frame of the STEP project, is based on a methodology, two features of which are addressed in detail: (1) the parameters of Omori's law and (2) application of attenuation relations in evaluating peak ground velocity exceedence probability. Concerning the first point, we perform a simple parametric study. We assume the generalized Omori's law by Shcherbakov et al. (Geoph Res Lett 31:L11613, 2004), in which characteristic time c scales with aftershock magnitude. The study shows that, among all the parameters, the hazard is most sensitive to the choice of m^* (controlling the overall aftershock productivity) and least sensitive to the scaling of c. We also conclude that the hazard is mainly due to very early (less than 1 day) aftershocks. As regards the second point, we employ various attenuation relations from different tectonic areas to study their effect on the hazard analysis. We conclude that the resulting variations are relatively large, comparable to those obtained for varying m^*.

Keywords Time-dependent aftershock probabilistic hazard · Aftershock statistics · Omori's law · Attenuation relations

F. Gallovič (✉) · J. Brokešová
Department of Geophysics,
Faculty of Mathematics and Physics,
Charles University, V Holešovičkách 2,
Prague 8, 180 00, Czech Republic
e-mail: gallovic@karel.troja.mff.cuni.cz

1 Introduction

In the seismic hazard assessment due to a possible aftershock, we encounter problems because a number of faults are designated to produce likely aftershocks, whose possible magnitudes are unknown. Moreover, the seismogenic zone can be capable of producing earthquakes due to slip on blind faults. In all these cases, the question arises of providing strong-ground motion prediction maps for all possible scenarios, including various magnitudes and likely activated fault zones, for responsible authorities. A possible approach is to combine all the predictions into a single, easy-to-understand map. Wiemer (2000) suggested the so-called probabilistic aftershock hazard assessment (PAHA), based on the classical probabilistic seismic hazard approach (PSHA, Cornell 1968). Its special form has been, for example, recently applied in the STEP program (available online since May 2005 at http://pasadena.wr.usgs.gov/step) for California (Gerstenberger et al.

2005), which provides the probability of strong shaking in California within the next 24 h. This paper, however, deals with the PAHA approach in a general sense.

PAHA intrinsically combines two main features: (1) the statistical description of aftershock occurrence and (2) the probability density function of the strong-motion characteristics under study [peak ground velocity (PGV) in our case] as a function of earthquake magnitude and station location. The latter is used to translate the aftershock probabilities to the probabilistic forecast of strong-motion characteristics exceedence.

As regards the first point, recently, there have been several attempts to assess aftershock occurrence. They are based either on physical models (e.g., using the rate-and-state friction law, Dieterich 1994) or statistical models, in which characteristics of the observed seismicity are used to infer the nature of future seismicity (Reasenberg and Jones 1989). One of the statistical models, used also in the STEP program, combines nonstationary Poisson process and the generalized Omori's law describing the aftershock mean occurrence rate (the time derivative of the number of occurring aftershocks), namely, its temporal decay and dependence on aftershock magnitude. In this respect, the aftershock hazard is intrinsically time-dependent in contrast to the classical PSHA (based on stationary Poisson process), where the hazard is time invariant.

Concerning PGV dependence on aftershock magnitude and station position, empirical attenuation relations are usually employed. Attenuation relations vary with the area under study, data employed, and method utilized by the author. Alternatively, empirical strong ground motion prediction can be substituted by simulations, which is discussed in the paper by Gallovič and Brokešová (2008) (further referred to as the companion paper).

In this paper, the aim is to test the general PAHA approach (not only its particular implementations, such as STEP). We first recapitulate the equations used in PAHA. Then we present a simple hazard parametric study (utilizing attenuation relations) focused on the parameters in Omori's law. Furthermore, we take into account several attenuation relations to illustrate their effect on the hazard.

2 Probabilistic aftershock hazard analysis

Because we are not able to predict the aftershock occurrence in terms of position and time exactly, a probabilistic approach has to be employed. Let us assume a region where a mainshock started an aftershock sequence. It is common to assume that the aftershock occurrence is a nonstationary Poisson process, so that we can write the probability that an aftershock of magnitude $m' \geq m$ will occur within time interval T_1 to T_2 (after the mainshock) as

$$P_1(T_1, T_2) = 1 - \exp\left(-\int_{T_1}^{T_2} r(m' \geq m, t)dt\right), \quad (1)$$

where r is the mean occurrence rate of aftershocks with magnitude $m' \geq m$ at time t. It is well known that rate r in a given area can be approximated by Omori's law, which suggests its temporal decay. Shcherbakov et al. (2004) introduce this law in the following, general form:

$$r(m' \geq m, t) = \frac{N(m' \geq m)(p-1)/c(m' \geq m)}{(1 + t/c(m' \geq m))^p}, \quad (2)$$

where $c(m' \geq m)$ is the characteristic time dependent on magnitude (see later). Parameter p controls mainly the time decay slope, i.e. whether the aftershocks tend to occur earlier after the mainshock (higher p) or later (lower p). $N(m' \geq m)$ is the total number of aftershocks of magnitudes $m' \geq m$, i.e., $N(m' \geq m) = \int_0^T r(m' \geq m, t)dt$ in the limit $T \to \infty$. Note that convergency of this limit is guaranteed only if $p > 1$.

Number $N(m' \geq m)$ can be described by the Gutenberg–Richter relation modified for aftershocks (Shcherbakov et al. 2004):

$$N(m' \geq m) = 10^{b(m^* - m)}. \quad (3)$$

Parameter b characterizes the number-size distribution of events (smaller b indicates more large

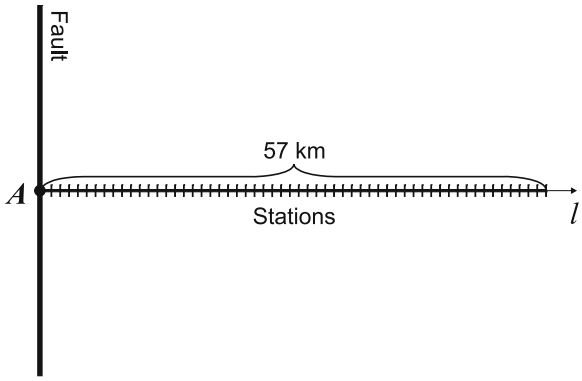

Fig. 1 Geometry for numerical testing of PAHA. The aftershocks are assumed to occur in the very center of the fault

events) and m^* controls the productivity of the area.[1]

Parameter c is the characteristic time for aftershocks of magnitudes $m' \geq m$. Shcherbakov et al. (2004) found a scaling relation for it,

$$c(m' \geq m) = c(m^*)10^{\beta'(m^*-m)}. \quad (4)$$

Quantity β' controls the ratio of characteristic times between higher and lower m's, $\beta' > 0$. If β' increases, the characteristic times for aftershocks of magnitudes $m < m^*$ increase, while for those of $m > m^*$ decrease. This, consequently, means that (with increasing β') small aftershocks tend to delay, while the large ones tend to occur earlier after the mainshock. Note that $\beta' = 0$ implies the characteristic time being independent of magnitude, which is assumed, e.g., in the STEP program in California.

Parameters m^*, b, p, β', and $c(m^*)$ are empirically observed parameters that can be estimated from previous or on-going aftershock sequences. Their values are briefly discussed in the next section, where we also study the influence of the parameter variations on aftershock hazard.

Let us assume a mainshock followed by an aftershock sequence triggered on a given fault with its center at position $\boldsymbol{A}$. For the sake of simplicity, let us assume that the aftershocks occur just in the center of the fault ($\boldsymbol{A}$). Furthermore, we consider simple fault-station geometry as shown in Fig. 1. Stations are located on the profile perpendicular to the fault and passing through $\boldsymbol{A}$. Their position is measured by distance l, $l = ||\boldsymbol{A} - \boldsymbol{x}||$.

The quantity of our main interest in the PAHA is the probability of exceedence of certain strong-motion characteristics. Generally, any strong-motion characteristic can be studied. In this paper, for the sake of brevity, we restrict ourselves to the PGV. The probability of PGV value v exceedence at receiver at distance l during time interval T_1 to T_2 can be written as

$$P_v(l, T_1, T_2) = 1 - \exp\left(-\int_{T_1}^{T_2} \Lambda(v' \geq v, l, t)dt\right), \quad (5)$$

where Λ is the rate of $v' \geq v$ occurrence. It can be obtained by integration

$$\Lambda(v' \geq v, l, t) = \int_{m_{min}}^{m_{max}} \frac{dr}{dm}\lambda(v' \geq v, l, m)dm, \quad (6)$$

where r is given by Eq. 2, taking into account Eqs. 3 and 4. Quantity $\lambda(v' \geq v, l, m)$ represents probability of $v' \geq v$ occurrence at distance l from magnitude m event. Note that a more general formula taking into account spatial distribution of possible sources can be found in our companion paper.

The PGV distribution is usually assumed to be log-normal in regression of attenuation relations, being described by quantities $\bar{v}(l, m)$ and $\sigma(l, m)$. Therefore, we can write

$$\lambda(v' \geq v, l, m) = \frac{1}{\sqrt{2\pi}\sigma(l, m)} \times \int_{\ln v}^{\infty} \exp\left[-\left(\frac{\ln v' - \ln \bar{v}(l, m)}{\sqrt{2}\sigma(l, m)}\right)^2\right] d(\ln v'). \quad (7)$$

In this way, $\ln \bar{v}$ and σ correspond to the mean and standard deviation of logarithms of PGVs, respectively.

[1] In the paper by Shcherbakov et al. (2004), m^* is introduced as the magnitude of the "largest" aftershock inferred from an extrapolation of the Gutenberg–Richter relation because $N(m' \geq m^*) = 1$ (see Eq. 3). Note that m^* is defined formally and does not correspond to the magnitude of the real largest aftershock of the sequence under study.

Table 1 Parameters obtained for five Californian earthquakes (Shcherbakov et al. 2004, 2006)

Earthquake	m_{ms}	m^*	b	p	β'	$c(m^*)$ [s]
Landers	7.3	6.20 ± 0.05	0.98 ± 0.02	1.22 ± 0.03	1.0 ± 0.4	33 ± 10
Northridge	6.7	5.95 ± 0.05	0.91 ± 0.02	1.18 ± 0.02	0.8 ± 0.7	23 ± 10
Hector Mine	7.1	5.75 ± 0.05	1.01 ± 0.01	1.21 ± 0.05	1.1 ± 0.6	32 ± 10
San Simeon	6.5	5.40 ± 0.05	1.00 ± 0.03	1.12 ± 0.02	0.8 ± 0.8	55 ± 10
Parkfield	6.0	5.00	0.89 ± 0.01	1.09 ± 0.02	0.7 ± 0.3	15 ± 1

Symbol m_{ms} denotes the mainshock magnitude

To obtain the probabilities as a function of fault distance for given aftershock sequence statistic parameters and attenuation relations, we insert Eqs. 7 and 6 into Eq. 5. From the computational point of view, the differentiation dr/dm and integration over t are performed analytically, while the integration over m numerically, i.e., replacing the integral by a sum. The bounds m_{min} and m_{max} in Eq. 6 are such that the resulting probabilities P_v do not change substantially if they are slightly decreased or increased, respectively.

3 Numerical testing of PAHA sensitivity to parameters of the generalized Omori's law

In this section, we investigate numerically the sensitivity of PAHA to the above-described statistical parameters, namely dimensionless parameters m^*, b, p, β', and characteristic time $c(m^*)$, for several time ranges after a hypothetical mainshock. We assume a mainshock of magnitude $m_{ms} = 6.5$. We discuss the sensitivity on plots (further referred to as hazard plots), showing the probabilities of exceeding $v = 0.1$ m/s with respect to the fault distance. The 57 virtual receivers are distributed with 1 km spacing over a range of 1–57 km; see Fig. 1.

In this section, we employ the attenuation relations by Si and Midorikawa (1999). Note that this choice is arbitrary because our parametric study is general, not specific to any region. In the next section, we also investigate the effect of the choice of particular attenuation relations on the probabilities.

The variability of the above-mentioned statistical parameters may be relatively large. To assume reasonable ranges of the parameters, we utilize past aftershock sequences, for which the statistical parameters have been determined in previous studies. An extended review by Utsu et al. (1995) has discussed p value variability of instrumentally observed sequences, and they have found the range between 0.8 and 1.4. Wiemer et al. (2002) have found spatial variability of b and p during the 1999 Hector Mine aftershock sequence in the range of 0.7–1.5 and 0.9–1.4, respectively. For Italy, Lolli and Gasperini (2003) have retrieved $p = 0.93 \pm 0.21$ and $b = 0.96 \pm 0.18$. The other parameters, m^*, $c(m^*)$, and β', have been inferred for five Californian aftershock sequences by Shcherbakov et al. (2004, 2006); see Table 1.

From the above discussion, it follows that the variability of the parameters may be relatively significant and possibly site-dependent. For our parametric study, we choose the ranges of the parameters as wide to cover all the above-discussed typical ranges of the parameter values; see Table 2. Note that, as regards the p value, in our formulation we are restricted to $p > 1$ (due to the finiteness of the integral of modified Omori's law, Eq. 2). In the hazard plots that follow, we vary just one of the parameters while keeping the

Table 2 Ranges of aftershock statistic parameters under study

Parameter	Min	Reference value	Max
m^*	5.1	5.4	5.7
b	0.8	1.1	1.4
p	1.05	1.25	1.45
β'	0.0	1.0	2.0
$c(m^*)(s)$	15	30	60

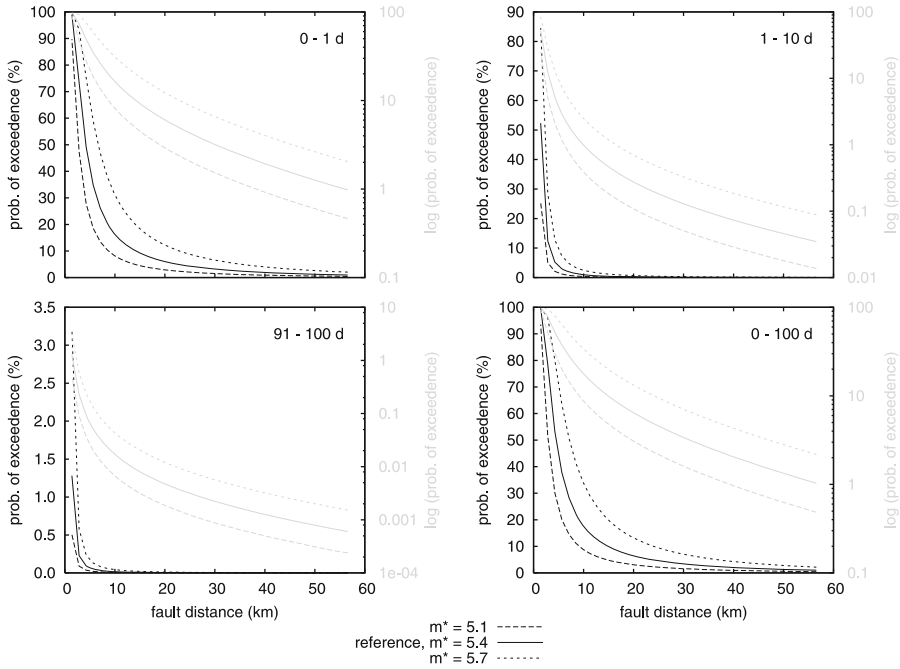

Fig. 2 Probabilities of exceeding PGV $v = 0.1$ m/s as a function of fault distance (l in Fig. 1) in normal (*black curves*) and logarithmic scales (*gray curves*). The four *panels* differ in time range considered (see labels). The *solid line* in all the plots corresponds to the reference setting: $m^* = 5.4$, $b = 1.1$, $p = 1.25$, $\beta' = 1.0$, and $c(m^*) = 30$ s. Parameter m^* is then varied, taking the values 5.1 and 5.7 (*dashed curves*)

others constant at so-called reference values (centers of the parameter's ranges), namely, $m^* = 5.4$, $b = 1.1$, $p = 1.25$, $\beta' = 1.0$, and $c(m^*) = 30$ s. Note again that the choice of parameters is not intended to be specific for any area. The integration bounds in Eq. 6 are set $m_{min} = 3.0$ and $m_{max} = 7.0$.

In Figs. 2, 3, 4, 5, and 6, we show the probability of exceeding $v = 0.1$ m/s as a function of fault

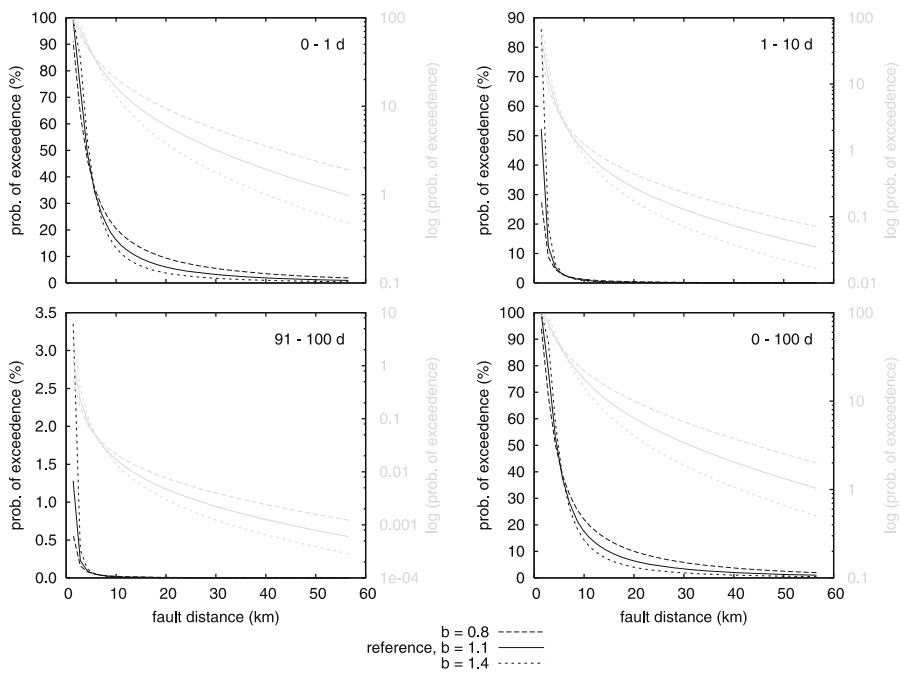

Fig. 3 Same as Fig. 2 but for parameter b variations in the range 0.8–1.4

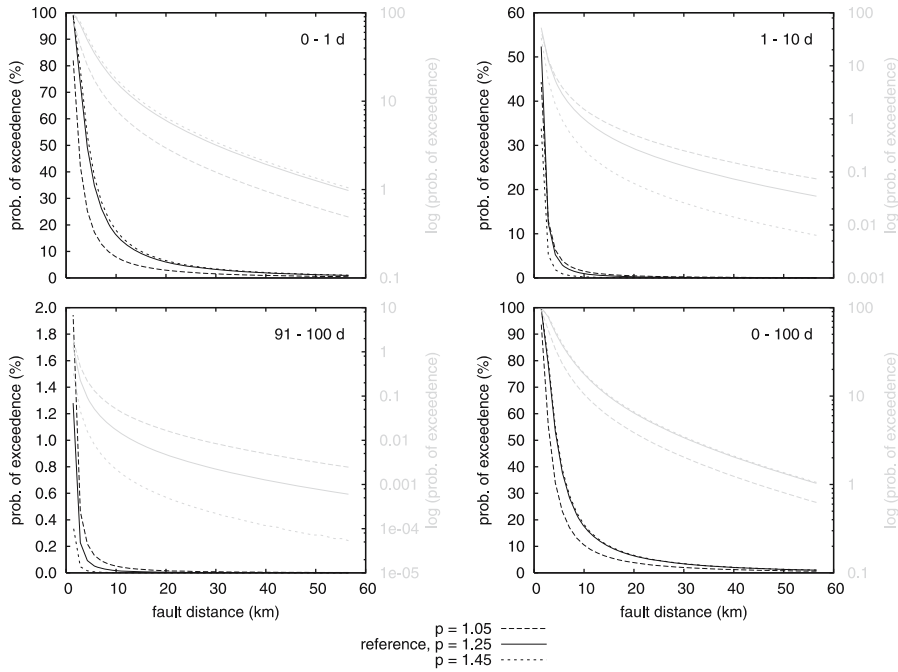

Fig. 4 Same as Fig. 2 but for parameter p variations in the range 1.05–1.45

distance for the variations of the individual parameters (namely, m^*, b, p, β', and $c(m^*)$). Each of the figures consists of four panels showing the probabilities for different time intervals:[2] the top left corresponds to the first day after the mainshock; the top right to the period 1–10 days; the bottom left to 91–100 days; and, finally, the bottom right to the whole period 0–100 days after the mainshock. The plots are displayed on both normal (black) and logarithmic scales (gray). While the first provides a better insight into the resulting absolute variations of the probabilities, the last enables us to see better their relative variations.

Let us first discuss the reference solution in Figs. 2–6 (which is the same in all the figures) for different time periods. As expected, the probability decreases with increasing fault distance. Further, at any fault distance, the probability also considerably decreases for later time ranges. This is clearly due to the time decrease of the aftershock rate in Omori's law that governs the hazard. For example, 5 km away from the fault, the probability drops from about 50% during the first day to 5% during the period 1–10 days (although being longer in time) and to 0.2% for the late period 91–100 days. However, the temporal decay is different at different fault distances. To get a better notion, Fig. 7 shows a 3D plot, where differential probabilities for time intervals of 1 day are plotted vs time delay T after the mainshock and fault distance. By differential probabilities, we understand difference $\Delta P_v(l, 0, T) = P_v(l, 0, T) - P_v(l, 0, T-1)$, with T being in units of days. Note that, in this way, $\Delta P_v(l, 0, T)$ are not probabilities of aftershock occurrence within the given day. The graph of differential probabilities ΔP_v in Fig. 7 shows that the temporal decay of P_v is fastest for short fault distances, as well as for smaller times after the mainshock.

Analyzing the probability behavior when changing the statistic aftershock sequence parameters in Figs. 2–6, we see that the probabilities are most sensitive, in the sense of the largest scatter, to variations of parameter m^* (see Table 2) in Fig. 2. This is due to the fact that this parameter controls the overall aftershock productivity. Except for the closest distances, for all the investigated time periods, the absolute scatter decreases while the relative one (see

[2]The time intervals are chosen to best accomplish the parametric study, regardless of our opinion of whether they are reasonable from the practical point of view.

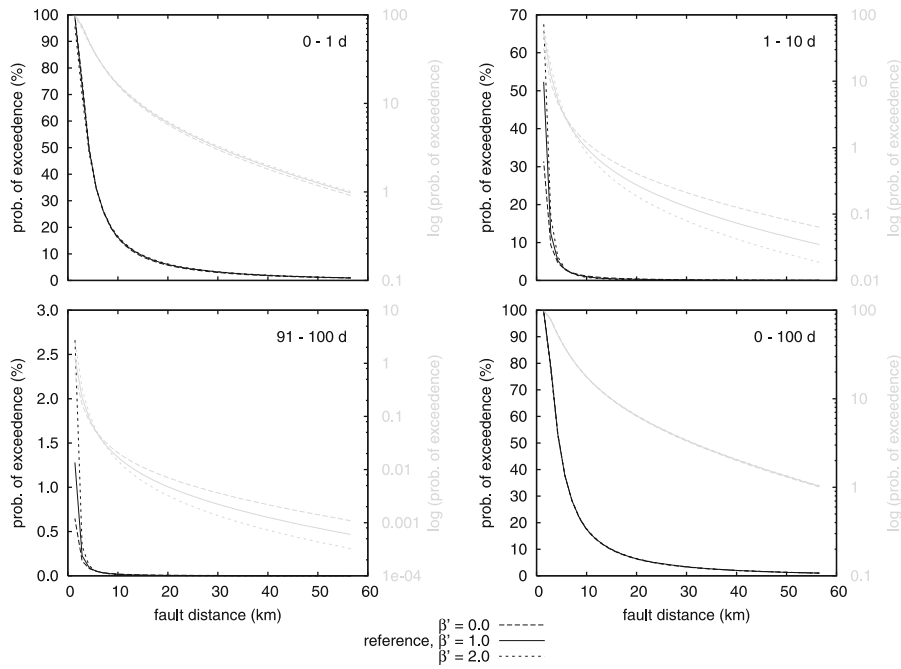

Fig. 5 Same as Fig. 2 but for parameter β' variations in the range 0.0–2.0

the logarithmic plots) remains approximately constant.

Concerning the b value of the Gutenberg–Richter relation, this influences the hazard plots much less (Fig. 3) than parameter m^*. While m^* affects the probabilities in the same way at all distances (i.e., the larger m^*, the higher the probabilities), b does not. For all time intervals considered, at distances smaller than about 5 km, a higher b value provides higher probabilities

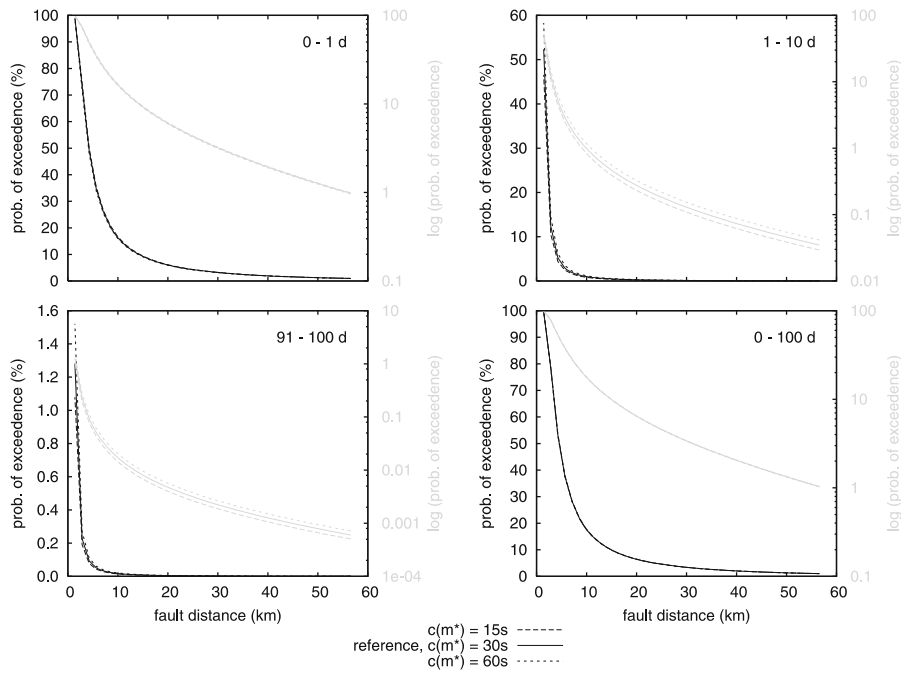

Fig. 6 Same as Fig. 2 but for parameter $c(m^*)$ variations in the range 15–60 s

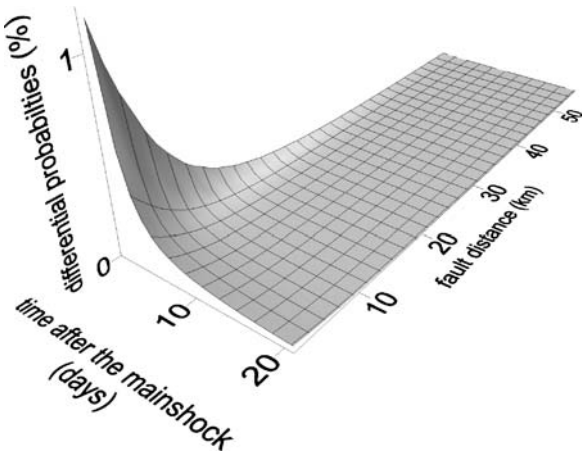

Fig. 7 Plot of 1-day differential probabilities with respect to the fault distance (l in Fig. 1) and time T after the mainshock. The term differential probabilities refers to the difference between probabilities obtained for time periods from 0 to T and from 0 to $T-1$, T being in units of days

(as in the case of m^*), while at larger distances, the opposite applies. We explain this as follows: higher b means a larger portion of small earthquakes that influence, in terms of ground motions, shorter distances. Beyond a particular distance, the influence starts being dominated by larger aftershocks. However, because there is a lower number of such large aftershocks for higher b (with respect to lower b), the probabilities at larger distances are lower.

As regards the variations of the p value in Omori's law (see Table 2), we can see in Fig. 4 that, in the time interval 0–1 day, the probabilities are higher for higher p, i.e., when aftershocks tend to occur earlier after the mainshock. For the intervals of 1–10 days, as well as 91–100 days, p influences the probabilities in the opposite way: the higher p, the lower the probabilities. The explanation is analogous as above because the aftershocks tend to occur earlier with increasing p; the probabilities are lower for the later intervals.

Varying β' (Table 2, Fig. 5), the plots exhibit a qualitatively similar behavior of the curves to the plots in which the b value varies (Fig. 3) including crossing of the curves. However, the overall variations would be less significant if one considers the first day after the mainshock. Moreover, looking closer to the case of the 0–1-day interval and at distances larger than about 7 km, the probabilities are higher for higher β', while for later times, the opposite applies. This is so because the scaling of the characteristic time (governed by parameter β') also affects the ratio between large and small aftershocks that change, however, with time. Higher β' means shorter characteristic time for larger magnitudes (see Eq. 4). Consequently, for the 0–1-day hazard plot, large earthquakes (affecting hazard at larger fault distances) tend to occur earlier after the mainshock than the small ones, which results in higher probabilities at larger distances. Further, during 1–10 days, the occurrence rate of larger aftershocks (with respect to the small ones) decreases, so that the hazard is dominated by small aftershocks that increase the probabilities at shorter fault distances.

Finally, the variations of parameter $c(m^*)$ (see Table 2) do not almost affect the probabilities when considering the first day after the mainshock; see Fig. 6 (upper-left and bottom-right panels). For later periods, 1–10 and 91–100 days, the influence of the variations is visible, but the scatter is the least when considering variations of the other parameters. In other words, the probability of exceeding $v = 0.1$ m/s is least sensitive to $c(m^*)$ from all the other statistic parameters.

Comparing the hazard plots in Figs. 2–6 for the interval of 0–100 days after the mainshock with the plots for the interval of 0–1 day, we conclude that the results are almost the same. Such similarity suggests that the hazard is mainly due to very early (less than 1 day) aftershocks.

4 Numerical testing of PAHA sensitivity to attenuation relations

In this section, we test the sensitivity of PAHA to the choice of attenuation relations derived by various authors for various areas. We employ those by Si and Midorikawa (1999), Atkinson (2006), and Skarlatoudis et al. (2003). The coefficients describing the relations, such as those related to source mechanism (strike-slip), soil type (hard rock), etc., are chosen in such a way to make the curves comparable. Figure 8 shows mean attenuation curves for a given magnitude, namely for the reference magnitude $m^* = 5.4$ from the last section. As one can see, the curves behave differently with dis-

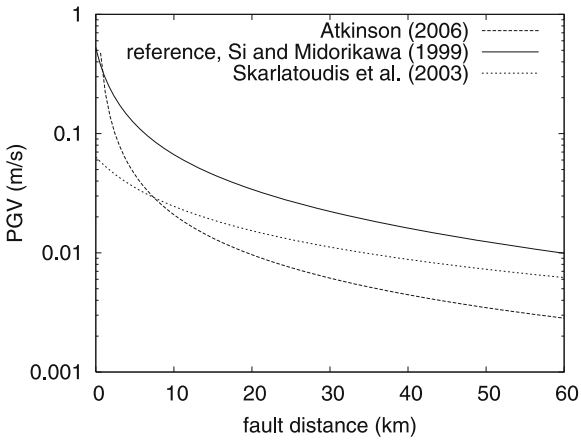

Fig. 8 An example of attenuation curves retrieved by various authors for reference magnitude $m^* = 5.4$

tance, which is mainly due to both different data employed and regression techniques utilized.

Figure 9 displays hazard plots for the reference values of the Omori's law parameters ($m^* = 5.4$, $b = 1.1$, $p = 1.25$, $\beta' = 1.0$, $c(m^*) = 30$ s) employing the above mentioned attenuation relations. By hazard plots, we again mean the probabilities of exceeding $v = 0.1$ m/s plotted with respect to the fault distance as in the last section (with the same source-station geometry, see Fig. 1). The time intervals are also the same as in the last section. The probabilities are again shown on both normal (black) and logarithmic scales (gray).

As expected, the variations in the probabilities for different attenuation relations vary considerably due to relatively large differences among the attenuation curves (see Fig. 8). This holds for all selected time intervals. Their scatter is comparable to that for variations in m^* (Fig. 2). Notwithstanding the large scatter, the decay of the probabilities with distance (see the logarithmic scale) is similar for the attenuation relations by Si and Midorikawa (1999) and Skarlatoudis et al. (2003). The probabilities for the attenuation relations of Atkinson (2006) are characterized by considerably faster decay at short epicentral distances. Despite the fact that the hazard curves are influenced by the attenuation relations' dependence on magnitude, this clearly reflects the fast distance decay of the attenuation curve itself at short distances (Fig. 8).

The dependence of attenuation relations on magnitude is manifested also by the different behaviors between probabilities obtained by the use of attenuation relations by, e.g., Atkinson (2006) and Skarlatoudis et al. (2003). Due to $\beta' > 0$,

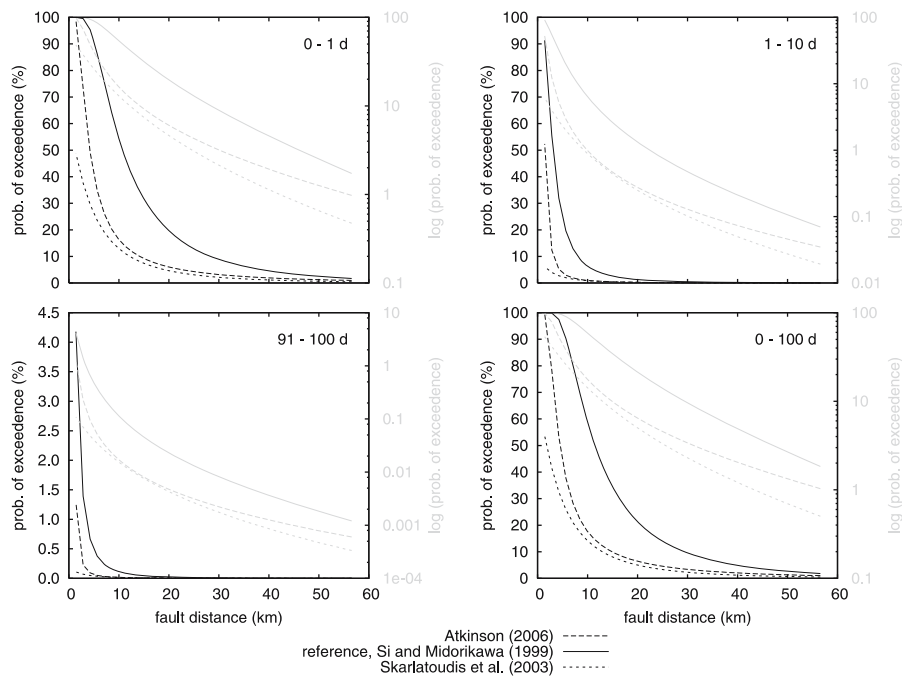

Fig. 9 Same as Fig. 2 but for variations of attenuation relations employed (see also Fig. 8)

the ratio between the number of large and small aftershocks depends on time interval selected. In this way, for time intervals 1–10 and 91–100 days, the curves (accidentally) touch each other, while, for time intervals 0–1 and 0–100 days, they do not (see also the discussion about the effect of β' in the last section). If we plot the hazard plots for $\beta' = 0$, the relative behavior among the curves would be the same for all time periods. Finally, note that, similarly to Figs. 2–6, the plots for the interval of 0–100 days after the mainshock are almost the same as for the interval of 0–1 day, suggesting dominance of very early (less than 1 day) aftershock hazard.

5 Discussion and conclusions

Statistical occurrence of aftershocks is represented by the nonstationary Poisson process. This implies that the aftershock hazard is time-dependent, in contrast to the classical PSHA by Cornell (1968), based on the stationary Poisson process, where the hazard is time-independent. Note that, locally, at a given time, the nonstationary Poisson process corresponds to the stationary Poisson process, however, with its mean rate decaying with time according to Omori's law. Generally speaking, any Poisson process is based on the assumption that, locally in time, the occurrence of an event is independent of other events. From the physical point of view, this is not true, but we assume that, from the statistical point of view, the interactions among aftershocks are so complex that aftershock occurrence appears to be independent and stochastic.

Note that Omori's law describes the aftershock rate decay well when stacked over many aftershock sequences. Rather, it does not reproduce the complex details of the individual sequences. Large aftershocks can, for example, significantly perturb this decay by increasing the seismicity rate on local faults. A more general approach to the probabilistic seismicity estimations is the epidemic-type aftershock sequence model proposed by Ogata (1988). This more sophisticated approach, however, relies on a number of parameters, the estimates of which are not always robust. This is particularly critical if the model is to be used as a forecast tool. Therefore, our studied PAHA (employing Omori's law) have to be understood as a forecast for a "typical" sequence (averaged over an ensemble of sequences) because the governing Omori's law is just a very good first-order approximation of a "typical" aftershock rate decay. After a strong aftershock (possibly close in magnitude to the mainshock) that significantly disturbs the aftershock rate, the PAHA can be reconsidered with updated Omori's law parameters (using actual aftershock seismicity data).

We provide a simple parametric study varying the parameters of the generalized Omori's law (Eq. 2), governing the time decay of the Poisson process mean rate. The ranges are chosen in such a way to cover typical values found by various authors for different aftershock sequences; see Table 2.

Regarding the p parameter (time decay exponent of the aftershock occurrence rate), we have limited it to $p > 1$ in our study. The p values lower than 1 are hard to be justified physically because this would lead to an infinite total number of aftershocks when time grows to infinity. One can of course object that the Omori's law controls the aftershock sequence only for a limited time. However, this would require the introduction of an additional temporal damping parameter for larger time intervals. Note that p values lower that 1 can be caused just by a bias during the regression of the seismicity data (due to the presence of background seismicity). Reformulation of the formulas related to the Omori's law would be straightforward.

Our study shows that the hazard is affected mainly by parameters m^* (extrapolated maximum aftershock magnitude), b (decay exponent in the Gutenberg–Richter relation), and p. Therefore, these parameters have to be precisely determined. This requirement is, however, difficult to meet very early after the mainshock because seismologists collect sufficient seismicity data within at least the first 3 days (Wiemer et al. 2002). On the other hand, as we have found, the absolute probabilities for later times are not so sensitive to the variations of statistical parameters, which makes the PAHA (for later times) very promising for real applications.

In areas without strong-motion networks and related infrastructure dense enough to analyze seismicity in real time, a preliminary spatial variation of the seismicity parameters can be found from available historical instrumental data (Lolli and Gasperini 2003). They can be then used to assess the hazard in the first few days after the mainshock before a reliable model of the ongoing sequence is available.

Generally, the hazard computation is usually based on empirically observed statistical parameters, which may be biased due to an incomplete data set. For example, values of c are derived based on a data set missing a number of aftershocks immediately after the mainshock, so that it is found larger than it should be. Kagan (2004) suggests a value of c close to zero. However, Utsu et al. (1995) conclude from high-resolution and corrected observations that actual c values are positive. Shcherbakov et al. (2006) argue that the positive c value depending on magnitude is a physical property. However, if the apparent c value results from incomplete aftershock detection, it should be decreased to obtain a more realistic hazard. Accordingly, the value of m^* has to be adjusted simultaneously to take into account the increased number of undetected aftershocks. The corresponding change in the hazard would then be governed mainly by the change in m^*, i.e., in the way shown in Fig. 2.

Regarding the detailed quantitative analysis of the hazard plots in Figs. 2–6, it depends, of course, on the reference values chosen in our study. We have made a lot of numerical tests with other reference values. According to our experience, for example, the crossing of probability curves in Figs. 3 and 5 would appear at larger distance when considering larger b and p values. However, the qualitative behavior of the curves in the hazard plots would remain the same.

The parametric study presented in this paper can be useful, for example, in other PAHA implementations, such as the STEP program. It has started operating in California as a real-time hazard forecast for the next 24 h (Gerstenberger et al. 2005). In that program, generic California attenuation relations and, in its first stage, generic California aftershock sequence parameters are considered. Our present study shows how sensitive the hazard is to the particular choice of the attenuation relations and the aftershock sequence parameters. Further, in the later stage of the STEP program, spatial variations of Omori's law parameters determined from the ongoing sequence are considered (Wiemer and Katsumata 1999). Our parametric study, showing the sensitivity of the PAHA probabilities to the seismicity parameters, suggests that such variations could be important for the hazard analysis. Moreover, Omori's law with constant characteristic time c (i.e., $\beta' = 0$) is employed in STEP. The value of β' is hard to determine because it requires a large amount of aftershock seismicity data. Our study shows that the choice $\beta' = 0$ is acceptable because the hazard is affected much more by the other parameters (m^*, b, p).

Another question in our study regards the use of attenuation relations for the translation from occurrence probabilities to the probabilities of exceedence. We have tested the sensitivity of PAHA to the choice of various attenuation relations and found that the influence is relatively large, being comparable to variations for different choices of m^*. On the other hand, attenuation relations employed in our study (Si and Midorikawa 1999; Atkinson 2006; Skarlatoudis et al. 2003) are perhaps rather diverse because they have been derived for different areas (Japan, USA, and Greece, respectively). Presumably, various attenuation relations for the same area (e.g., assuming a slightly different data set) would yield less different curves in the hazard plots. An alternative approach would be to utilize strong ground motion simulations to substitute the attenuation relations. This could be important especially in areas where the aftershocks are likely to occur at a given known fault and/or attenuation relations are not available (e.g., due to low data coverage). Such an approach is tested in our companion paper.

Acknowledgements Reviews of two anonymous referees helped to improve the manuscript. The research was supported by the Grant Agency of Charles University (292/2005/B-GEO/MFF), MSM 0021620800, the Grant Agency of the Czech Republic (205/07/0502), and the Marie Curie training network SPICE in the 6th Framework Program of the European Commission (MRTN-CT-2003-504267).

References

Atkinson GM (2006) Single-station sigma. Bull Seismol Soc Am 96:446–455

Cornell CA (1968) Engineering seismic risk analysis. Bull Seismol Soc Am 58:1583–1606

Dieterich J (1994) A constitutive law for rate of earthquake production and its application to earthquake clustering. J Geophys Res 99:2601–2618

Gallovič F, Brokešová J (2008) Probabilistic aftershock hazard assessment II: application of strong ground motion modeling. J Seismol, doi:10.1007/s10950-007-9070-2

Gerstenberger MC, Wiemer S, Jones LM, Reasenberg PA (2005) Real-time forecasts of tomorrow's earthquakes in California. Nature 435:328–331

Kagan YY (2004) Short-term properties of earthquake catalogs and models of earthquake source. Bull Seismol Soc Am 94:1207–1228

Lolli B, Gasperini P (2003) Aftershocks hazard in Italy Part I: estimation of time-magnitude distribution model parameters and computation of probabilities of occurrence. J Seismol 7:235–257

Ogata Y (1988) Statistical models for earthquake occurrences and residual analysis for point processes. J Am Stat Assoc 83:9–27

Reasenberg PA, Jones LM (1989) Earthquake hazard after a mainshock in California. Science 243:1173–1176

Shcherbakov R, Turcotte DL, Rundle JB (2004) A generalized Omori's law for earthquake aftershock decay. Geophys Res Lett 31:L11613, 5 pp

Shcherbakov R, Turcotte DL, Rundle JB (2006) Scaling properties of the parkfield aftershock sequence. Bull Seismol Soc Am 96:S376–S384

Si H, Midorikawa S (1999) New attenuation relationships for peak ground acceleration and velocity considering effects of fault type and site condition. J Struct Constr Eng AIJ 523:63–70

Skarlatoudis AA, Papazachos CB, Margaris BN, Theodulidis N, Papaioannou Ch, Kalogeras I, Scordilis EM, Karakostas V (2003) Empirical peak ground-motion predictive relations for shallow earthquakes in Greece. Bull Seismol Soc Am 93:2591–2603

Utsu T, Ogata Y, Matsu'ura RS (1995) The centenary of the Omori formula for a decay law of aftershock activity. J Phys Earth 43:1–33

Wiemer S (2000) Introducing probabilistic aftershock hazard mapping. Geophys Res Lett 27:3405–3408

Wiemer S, Gerstenberger M, Hauksson E (2002) Properties of the aftershock sequence of the 1999 Mw 7.1 Hector mine earthquake: implications for aftershock hazard. Bull Seismol Soc Am 92:1227-1240

Wiemer S, Katsumata K (1999) Spatial variability of seismicity in aftershock zones. J Geophys Res 104: 13135–13151